Draft version 2017/02/03
Preprint typeset using LaTeX style emulateapj v. 11/10/09

A CATALOG OF 3MM POINT SOURCES IN THE SGR B2 CLOUD: SIGNS OF EXTENDED STAR FORMATION IN A CMZ CLOUD

Adam Ginsburg[2,1],

[1] *National Radio Astronomy Observatory, Socorro, NM 87801 USA*
aginsbur@nrao.edu

Draft version 2017/02/03

ABSTRACT

We report the detection of > 100 sources in the Sgr B2 clouds with extents smaller than 5000 AU. These sources are most likely to be protostars or centrally condensed prestellar cores. The spatial distribution of these sources demonstrates that Sgr B2 is experiencing a highly extended star formation event, not just an isolated 'starburst' within the protocluster regions M, N, and S.

1. OBSERVATION AND DATA REDUCTION

Data were acquired as part of ALMA project 2013.1.00269.S. Observations were taken with the 12m Total Power array, the ALMA 7m array, and in two configurations with the ALMA 12m array. The setup included the maximum allowed number of channels, 30720, across 4 spectral windows in a single polarization; the single-polarization mode was adopted to support moderate spectral resolution across the broad bandwidth.

The ALMA QA2 calibrated measurement sets were combined to make a single high-resolution, high-dynamic range data set. We imaged the continuum jointly across all four bands, and found that the central regions surrounding Sgr B2M were severely affected by artifacts that could not be cleaned out. We therefore ran 3 iterations of phase-only self-calibration and one iteration of amplitude + phase self-calibration to yield a substantially improved image. The total dynamic range, measured as the peak brightness in Sgr B2 to the RMS noise in a signal-free region of the image, is 22000 (noise $\sim$ 0.08 mJy/beam), while the dynamic range within one primary beam ($\sim 0.5'$) of Sgr B2M is only 3700 (noise $\sim$ 0.5 mJy/beam). Because of the dynamic range limitations, and an empirical determination that clean did not converge if allowed to go too deep, we cleaned to a threshold of 0.5 mJy/beam across the image. We performed this same process for both the longest-baseline data only (resolution $\sim 0.5''$, largest angular scale theoretically $15''$ [the shortest baseline] but more practically $\sim 7''$ [the 5th percentile baseline length]) and the merged 7m + two 12m configuration data. The merged data are more useful for studying extended structures but have lower dynamic range, while the long-baseline-only data are excellent for extracting and analyzing pointlike or compact sources.

We also produced cubes of all of the spectral lines. These were lightly cleaned with only 200 iterations of cleaning. No self-calibration was applied. Before continuum subtraction, dynamic range related artifacts similar to those in the continuum images were present, but these structures are identical across frequencies, and were therefore removable in the image domain. We use median-subtracted cubes for the majority of our analysis, noting that the only location in which an error on the continuum > 5% is expected is the Sgr B2 North core (**?**).

2. ANALYSIS

2.1. *Continuum Source Identification*

We selected continuum point sources as candidate cores or protostars by eye. An automated selection is not viable across the majority of the field because there are many extended H II regions that dominate the overall map emission. A future automated selection algorithm may work if images at comparable resolution at other frequencies become availabe; the H II-region sources could then be excluded. Additionally, however, there are substantial imaging artifacts produced by the extremely bright emission sources in Sgr B2 M ($S_{3mm,max} > 0.8$ Jy) and Sgr B2 N ($S_{3mm,max} > 0.3$ Jy) that make automated source identification particularly challenging in the regions they are most common.

3. RESULTS

We detected 138 compact continuum sources. The majority of these are likely to be dust-dominated protostellar envelopes, though some are free-free dominated hypercompact H II regions. They are unlikely to be dusty prestellar cores, since they are predominantly unresolved or barely resolved, with $R < 1''$ ($R < 8500$ AU). Instead, most of these sources are likely to be protostellar cores with a central heating source and a dusty envelope.

3.1. *Source Classification*

We first note some key properties of dust at 3 mm. At 8.4 kpc, a 1 mJy source corresponds to an optically thin dust mass of $M(40\mathrm{K}) = 18\ M_\odot$ or $M(20\mathrm{K}) = 38\ M_\odot$ assuming a dust opacity index $\beta = 1.75$ to extrapolate the Ossenkopf & Henning (1994) opacity to $\kappa_{3mm} = 0.0018$ cm^2 g^{-1}. Our dust-only 5-σ sensitivity limit at 40 K therefore ranges from $M > 7\ M_\odot$ to $M > 45\ M_\odot$ across the map. If we were to assume that these are all cold, dusty sources, as is typically (and reasonably) assumed for local clouds, they would be extremely massive and dense, with the lowest measurable density being $n(40\mathrm{K}) > 3 \times 10^6$ cm^{-3} (corresponding to 7 $M_\odot$ in a $0.5''$radius sphere). Such extremes objects are possible, but since we have detected > 100 of these sources, it makes sense to evaluate other possibilities.

Some validation of the protostellar hypothesis comes from catalog matching. The Caswell et al. (2010) Methanol Multibeam Survey identified 11 sources in our observed field of view, of which 10 have a clear match in our catalog. Others of the sources have been identified with known H II regions from Gaume et al. (1995).

We compare our detected sample to that of the Herschel Orion Protostar Survey (HOPS; Furlan et al. 2016) in order to get a general sense of what types of sources we have detected. Figure 1 shows the HOPS source fluxes at 870μm scaled to 3 mm assuming a dust opacity index $\beta = 1.5$, which is shallower than usually inferred. The 870μm data were acquired with a $\sim 20''$ FWHM beam, which translates to a resolution $\sim 1''$ at 8.4 kpc, so our beam size is very similar to theirs. The HOPS sources are all fainter than the Sgr B2 sources. The brightest HOPS source would only be 0.2 mJy in Sgr B2, or about a 4-σ source - below our detection threshold even in the noise-free regions of the map. We can therefore conclude that the Sgr B2 sources are much more luminous and therefore massive protostars.

We could assume that the stellar mass is linearly proportional to the 3 mm continuum flux density to infer the instantaneous stellar fraction in the cloud. However, this assumption is immediately at odds with our expectations: the flux density distribution follows a powerlaw with slope $\alpha = 1.94 \pm 0.07$ (fitted with the MLE method of Clauset et al. 2007), far shallower than the $\alpha \sim 2.35$ expected for a normal IMF.

If we make the very simplistic assumptions that the sources we detect are all $L \gtrsim 2000\ L_\odot$ ($M \gtrsim 8 M_\odot$), we can infer the total stellar mass. Using a Kroupa (2001) mass function with $M_{max} = 200\ M_\odot$, 0.45% of the mass is contained in $M > 8 M_\odot$ stars. Using $M = 8 M_\odot$ as the lower-limit case for each source, the identified sources have total mass $M(>8) = 1800 M_\odot$. The total stellar mass implied is $M_{tot} = 3.9 \times 10^5\ M_\odot$. If we use the mean stellar mass for $M > 8\ M_\odot$, $\bar{M} = 21.1\ M_\odot$, then $M_{tot} = 1 \times 10^6\ M_\odot$.

3.2. *An examination of star formation thresholds*

Lada et al, and others, have proposed that star formation can only occur above a certain density or column density threshold[1]. In G0.253+0.016, very little star formation has been observed (Longmore et al. 2013; Johnston et al. 2014; Rathborne et al. 2015) despite most of the cloud existing above the locally measured column density threshold.

Since we have detected substantial ongoing star formation in the form of high-mass protostars and/or protostellar cores, we can assess where these stars form and whether the same (lack of) a threshold exists in Sgr B2. We therefore plot the column density distribution (flux distribution?) and overlay the cumulative distribution function of the background brightness around the cores.

Comparing Sgr B2 to G0.253, the majority of the Sgr B2 cloud is brighter and at higher column than G0.253. The presence of star formation in Sgr B2 nearly all occurs at a higher column than exists within G0.253 (Figure 3). The lack of SF in the brick is therefore consistent with the active SF in Sgr B2 and the CMZ's higher SF threshold is confirmed.

3.2.1. *Comparison to Lada, Lombardi, and Alves 2010*

In this section, we compare the star formation threshold in Sgr B2 to that in local clouds performed by Lada et al. (2010). They determined that all star formation in local clouds occurs above a column density threshold $M_{thresh} > 116\ M_\odot\ \mathrm{pc}^{-2}$, or $N_{thresh}(\mathrm{H_2}) > 5.2 \times 10^{21}\ \mathrm{cm}^{-2}$ assuming the mean particle mass is 2.8 amu (Kauffmann et al. 2008). We first note, then, that *all pixels* in our column density maps are above this threshold by *at least* a factor of 10.

However, the CMZ is 8.4 kpc away from us in the direction of our Galaxy's center, meaning there is a potentially enormous amount of material unassociated with the Sgr B2 cloud along the line of sight. This material may be as low as $5{\times}10^{21}\ \mathrm{cm}^{-2}$ or as high as $5{\times}10^{22}\ \mathrm{cm}^{-2}$. The latter value is approximately the lowest seen within our field of view and would imply that there is a perfect vacuum surrounding the dense gas in the Sgr B2 cloud. Even with the very aggressive foreground value of $5{\times}10^{22}\ \mathrm{cm}^{-2}$ subtracted, essentially the whole cloud exists above this threshold. We can therefore immediately rule out the possibility that there is a universal star formation column threshold, since a large fraction of the observed volume exhibits no hint at all of star formation activity.

-What kind of stars are we sensitive to? Are they?

REFERENCES

Caswell, J. L. et al. 2010, MNRAS, 404, 1029
Clauset, A., Rohilla Shalizi, C., & Newman, M. E. J. 2007, ArXiv e-prints
Furlan, E. et al. 2016
Gaume, R. A., Claussen, M. J., de Pree, C. G., Goss, W. M., & Mehringer, D. M. 1995, ApJ, 449, 663
Johnston, K. G., Beuther, H., Linz, H., Schmiedeke, A., Ragan, S. E., & Henning, T. 2014, A&A, 568, A56
Kauffmann, J., Bertoldi, F., Bourke, T. L., Evans, II, N. J., & Lee, C. W. 2008, A&A, 487, 993
Kroupa, P. 2001, MNRAS, 322, 231
Lada, C. J., Lombardi, M., & Alves, J. F. 2010, ApJ, 724, 687
Longmore, S. N. et al. 2013, MNRAS, 433, L15
Ossenkopf, V. & Henning, T. 1994, A&A, 291, 943
Rathborne, J. M. et al. 2015, ApJ, 802, 125

[1] Column density is more commonly used because of its observational convenience, but it is physically meaningless unless high column density leads to high optical depths and thereby changes the gas's ability to cool.

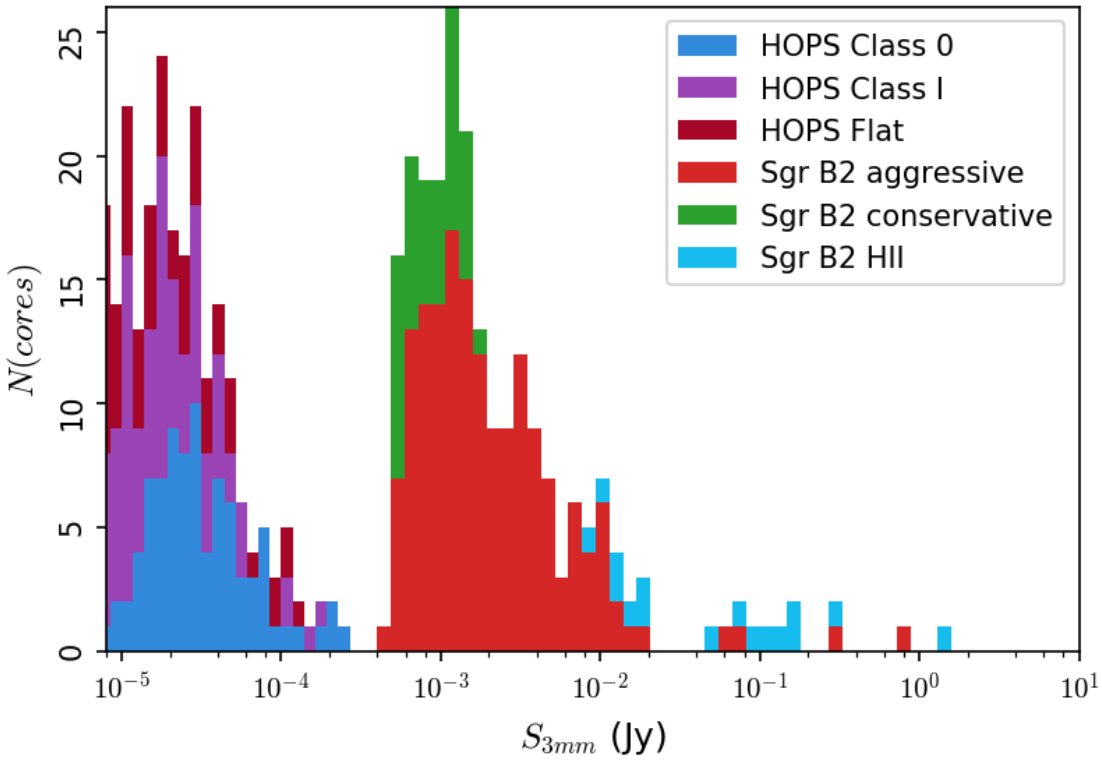

FIG. 1.— A histogram combining the detected Sgr B2 cores with predicted flux densities based on the HOPS (Furlan et al. 2016) survey. The HOPS histogram shows the 870 μm data from that survey scaled to 3 mm assuming $\beta = 1.5$. Every HOPS source is well below the detection threshold for our observations.

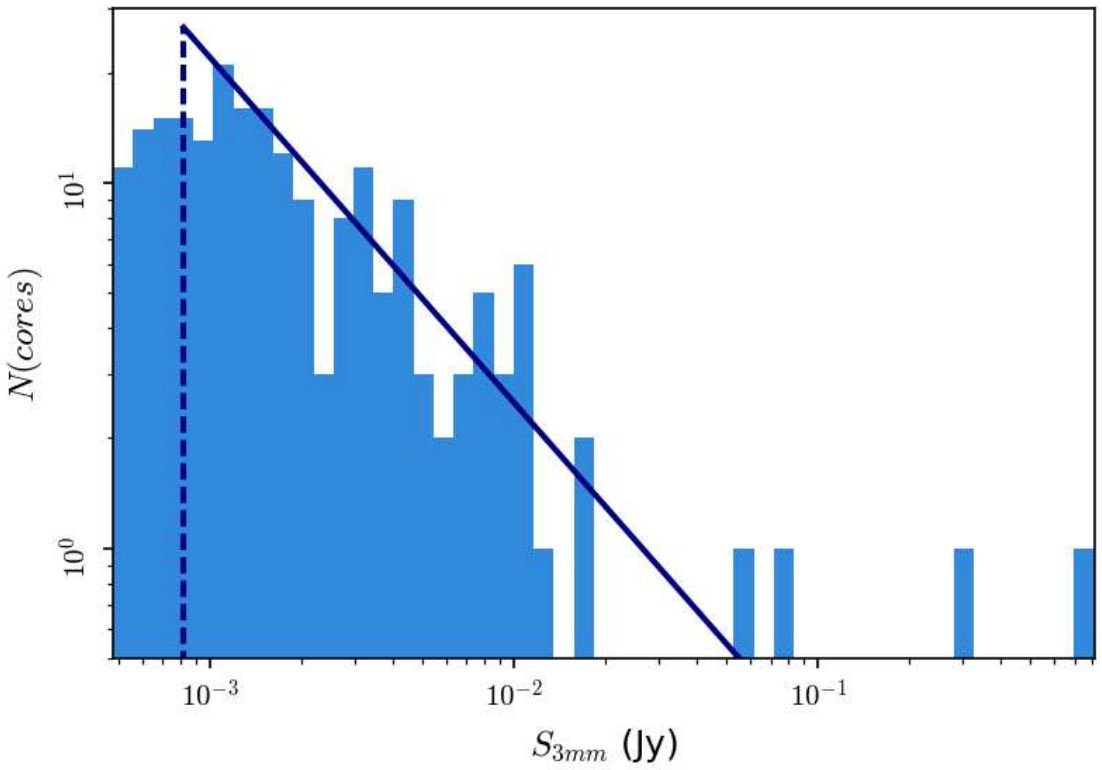

FIG. 2.— A histogram of the peak flux density of the observed sources excluding known H II regions with a powerlaw fit shown. The fitted powerlaw is an excellent fit to the data, but is far shallower than the IMF slope, with $\alpha = 1.94 \pm 0.07$. The two brightest regions are Sgr B2M f1 and Sgr B2N K2, which may be dominated by free-free emission but likely also contain a large dust mass.

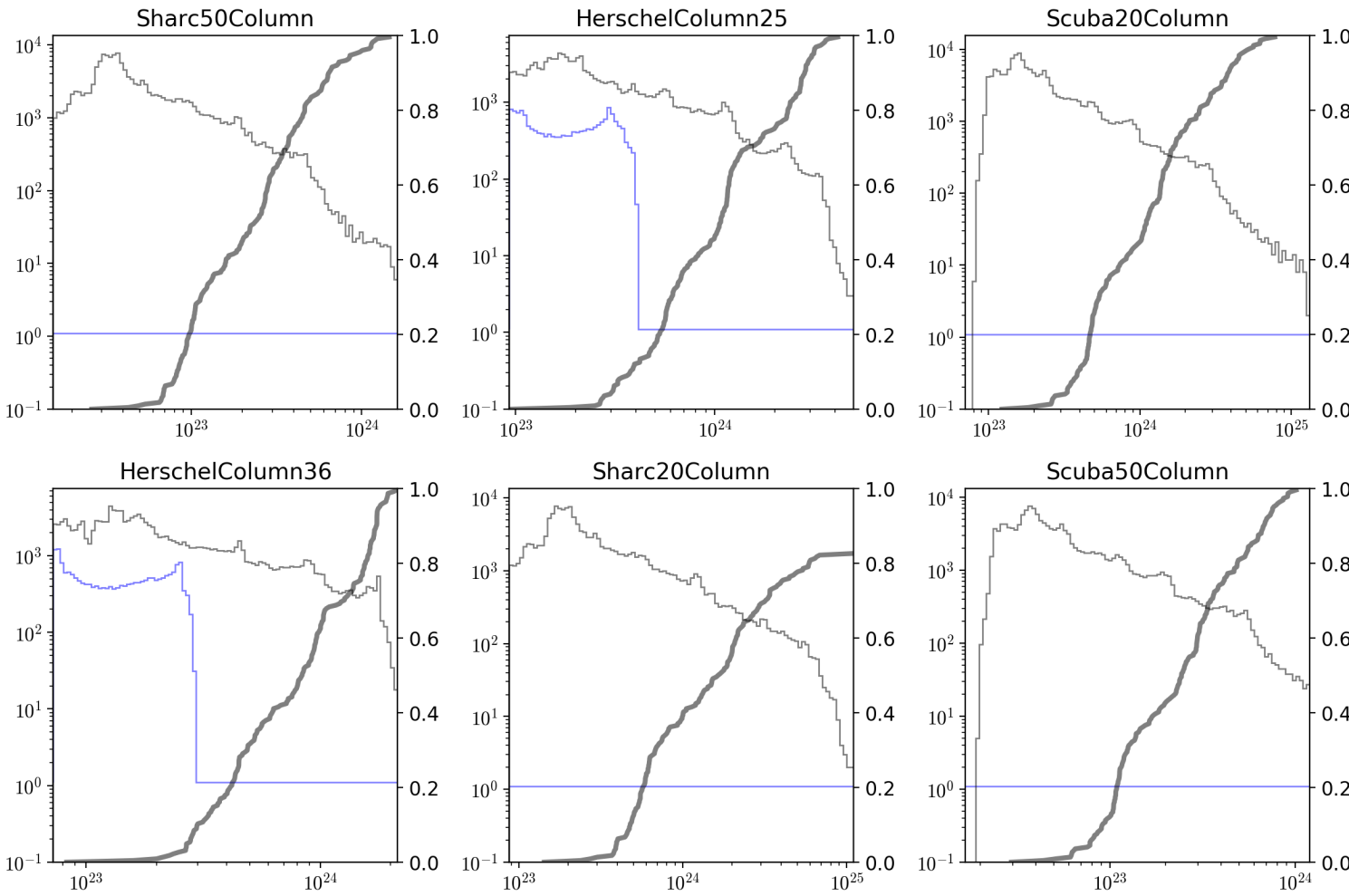

FIG. 3.— Histograms of the brightness measured with a variety of instruments at different submillimeter bands with the cumulative distribution function (CDF) of the *background* brightness surrounding each core superposed. The X-axis units are arbitrary (because right now I don't know the units of all of these) except for column, which is in units of cm^{-2} of H_2 as derived from SED fits to Herschel data (Battersby+). The grey line is of the observed region in Sgr B2 and the blue line is of G0.253+0.016. The thick grey line is the CDF of core background brightness, and is labeled by the right axis.